Variations of the Heppner-Maynard Boundaries on Northern Hemisphere Measured by SuperDARN During the Extremely Radial IMFs

Zhiwei Wang[1,2], Jianyong Lu[1], Hongqiao Hu[2], Jianjun Liu[2], Zejun Hu[2], Desheng Han[3], Ming Wang[1], Bin Li[2], Xiangcai Chen[2], Yewen Wu[1], Haiyan Guan[4]

[1]Institute of Space Weather, Nanjing University of Information Science and Technology, Nanjing, China
[2]MNR Key Laboratory for Polar Science, Polar Research Institute of China, Shanghai, China
[3]State Key Laboratory of Marine Geology, School of Ocean and Earth Science, Tongji University, Shanghai, China
[4]School of Remote Sensing & Geomatics Engineering, Nanjing University of Information Science and Technology, Nanjing, China

Corresponding author: Jianyong Lu (jylu@nuist.edu.cn)

Key point

- The averaged HMB midnight latitude driven by radial IMF is measured.
- The seasonal variation of B_X-HMB correlation coefficients is different with the existence of single lobe reconnection.
- The radial IMF effects on the S-M-I coupling sometimes should not be ignored, especially for the anti-sunward periods during the wintertime.

Abstract

The Heppner-Maynard Boundary (HMB) represents the equatorward extent of the ionospheric convection pattern and can be used as a proxy for the low latitude of the auroral oval. We present a statistical study of the radial interplanetary magnetic field (IMF) effects on the HMB midnight latitude calculated from SuperDARN measurements between January 2002 and December 2017. We found the average values of HMB midnight latitude during both sunward and anti-sunward radial IMF are higher than 65.5°. There is a negative correlation between the magnitude of B_X and HMB midnight latitude, although this effect is not obvious. Moreover, the seasonal variation of B_X-HMB correlation coefficients is different with the existence of single lobe reconnection. At the anti-sunward radial period, the correlation coefficient is up to 0.54 in wintertime. It would be caused by the enhanced lobe reconnection rates, which related to the special configuration between the solar-wind and magnetopause. This is the first long-term statistical study focused on HMB during radial IMF conditions in the context of solar wind-magnetosphere-ionosphere coupling. The results suggest that the effect of IMF B_X should not be ignored in the northern hemisphere wintertime especially during the anti-sunward radial IMF conditions.

Keywords: radial IMF, Heppner-Maynard Boundary, IMF B_X, S-M-I coupling

Plain Language Summary

The magnetic reconnection between solar wind and magnetosphere can drive a convection structure in the high-latitude ionosphere. Heppner and Maynard developed a method to calculate the equatorward boundary of the ionospheric convection, which is called Heppner-Maynard Boundary (HMB). HMB provides an import clue on solar wind-magnetosphere-ionosphere coupling. In this paper, we report the effects of the radial interplanetary magnetic field (IMF) on HMB in northern hemisphere. Our statistical results indicate that there is a negative and weak correlation between the strength of IMF B_X and HMB magnitude at midnight. The existence of reconnection happened on northern hemispheric high-latitude magnetosphere can affect the IMF B_X-HMB correlation coefficients, and also makes seasonal variation of coefficients different. Moreover, the effect of IMF B_X should not be ignored in northern hemisphere winter time during the negative radial IMF conditions.

1. Introduction

The solar wind-magnetosphere-ionosphere (S-M-I) coupling controlled mainly by the magnetic reconnection occurring at the dayside magnetopause and in the magnetotail is a key issue in space physics. It is well-known that the interplanetary magnetic field (IMF) B_Z component, which plays a crucial role in the reconnection rates and energy transmission from the solar wind to the magnetosphere. For southward IMF B_Z, large energy input could occur on the dayside magnetopause due to the low latitude reconnection between the IMF and the geomagnetic field (Akasofu, 1981; Dungey, 1961; Lu et al., 2013). During northward IMF, the energy and mass input is typically thought to be low (e.g., Lu et al., 2013). The amount of the open magnetic flux is modulated by the dynamic reconnection processes. The open-closed field line boundary (OCB) which is a surrounding region also called polar cap is the interface between geomagnetic field lines that are open to solar wind and closed to the opposite hemisphere (e.g., Lockwood, 1998; Rae et al., 2004; Kabin et al., 2004; Wang et al., 2014). The latitudinal location and movement of the OCB is of importance as it reflects the balance of magnetic reconnection on the magnetopause and in the magnetotail, and thus, reveals information about the total amount of open magnetic flux in the magnetosphere (Milan et al., 2007; Lu et al., 2019).

A function can describe the rate of expanding-contracting polar cap paradigm (ECPC) at a given time (Imber et al., 2013a, 2013b) :

$$\frac{dF_{PC}}{dt} = \Phi_D - \Phi_N = \frac{d}{dt}\int_{PC} \mathbf{B} \cdot dS \qquad (1)$$

where F_{pc} depicts the open magnetic flux in the polar cap, Φ_D marks the dayside reconnection rate, ϕ_N is the reconnection rate in the nightside, the ionospheric magnetic field vector is represented by B, and the integral is taken over the polar cap area. This function suggests that the reconnection in the dayside makes the polar cap expand and the reconnection in the magnetotail makes the opposite change. Therefore, the dynamic balance between the reconnections occurring in dayside and nightside is kept by a phenomenon known as steady magnetospheric convection. The observations of 25 nightside reconnection events provide evidence for the dynamic changes (Milan et al., 2007).

While direct measurement of Φ_N is difficult, many studies focus on Φ_D. Kan & Lee (1979) gives an early function:

$$\Phi = B_S V_S \left(\frac{\theta}{2}\right) l_0 \qquad (2)$$

where Φ represents the polar cap potential as an approximation of Φ_D, B_S marks the IMF southward component, V_S depicts the plasma inflow speed, Θ is the IMF clock angle, and$l_0 = 7R_E$, representing the effective length of the reconnection site. In other studies, B_S can be replaced by B_T or B_{YZ}(it is noticed that here B_T represents the modulus of the B_Y and B_Z components rather than B total. $B_{YZ}^2 = B_Y^2 + B_Z^2$) (Borovsky E., 2008; Milan et al., 2012; Newell et al., 2007; Scurry & Russell, 1991; Temerin & Li, 2006; Vasyliunas et al., 1982; Wygant et al., 1983). In these previous studies, the contribution of IMF B_X was not taken into account in the S-M-I coupling. Even in widely used MHD models, such as SWMF/BATS-R-US provided by Community Coordinated Modeling Center (CMCC), B_X can only be set to 0 or a constant (e.g., (Rae et al., 2004; Raeder et al., 2001; Wang et al., 2014; Lu et al., 2019) to avoid the non-zero magnetic field in the outer boundary.

As mentioned above, previous works completely ignored the contribution of B_X on the S-M-I coupling process. However, Belenkaya (1998) found that the ionospheric convection patterns changed with the angle of IMF in the X-Z plane, which was depended on 4 different topological structures between solar wind and magnetosphere. Other studies indicated that B_X can affect the asymmetry of reconnection for large scale coupling system (e.g., Peng et al., 2010; Tang et al., 2013). In addition, B_X will be transformed into the magnetosheath field B_Z with different polarities in the southern and northern hemispheres during radial IMF($|B_X|B_t$ ≥0.9) (Pi et al., 2017). There is no doubt that this change in direction can affect magnetic reconnection rates. A radial IMF, which is dominated by B_X, is a special and stable period of IMF normally with low plasma density, low velocity, low temperature, low dynamic pressure, and weak magnetic field (Pi et al., 2014). Radial IMF periods account for an important duration of total time (~16% for purely radial IMF periods and 10-15% for long periods larger than 4h) (Suvorova et al., 2010; Pi et al., 2014). Here, we aim to find out the relationship between radial IMFs and large scale S-M-I coupling, and when B_X effect has to be considered in the coupling.

The Heppner-Maynard Boundary (HMB) represents the equatorward extent of the ionospheric convection pattern. The characteristic shape of the boundary is determined by Dynamics Explorer 2 (DE2) electric field data (Heppner & Maynard, 1987) and is pole centered. That means the size of the boundary can be represented by the latitude at HMB midnight. For a large amount of statistical studies based on good Super Dual Auroral Radar Network (SuperDARN) data coverage, the HMB midnight latitude could be used as a proxy for the latitude of the auroral oval in the northern hemisphere (Boakes et al., 2008; Imber et al., 2013b). HMB is calculated by combining ionospheric model data (excluding B_X) with SuperDARN observation (including B_X). In this way, the influence of B_X on auroral oval can be revealed by HMB indirectly. In this study, we focus on radial IMF events and study the relationship between HMB measured by SuperDARN and B_X. That is, in our events, B_X dominates IMF with almost zero B_Y and B_Z components. This kind of parameter induces a very pure IMF B_X condition, thus the interferences that come from B_Y and B_Z components are eliminated effectively.

2. Data source and methodology

In this work, IMF data is obtained from the OMNI database. Previous works have demonstrated that, following a change of the IMF, 20 min is long enough to produce a reconfiguration for the magnetosphere-ionosphere (M-I) coupling system (Murr & Hughes, 2007; Grocott & Milan, 2014). Here we also choose 20 mins as the minimum timescale in this study. Radial IMF durations of 20, 30, 40, 50, 60 and 90 mins are selected as time bins, in each bin the radial IMF duration should be $\geq 90\%$ time of bin. This criterion means that, for 40 mins' time bin, the total radial time is 36 mins at least. For SuperDARN data, the ionospheric echoes from polar cap and high-latitude SuperDARN radars are considered as the database. Thomas & Shepherd (2018) shown that under the stronger solar wind driving condition, the inclusion of mid-latitude radar data at the equatorward extent of the ionospheric convection can increase the measured cross-polar cap potential (Φ in function 2) by 40%, but the increase is very small for weak solar wind driving condition. To keep the same SuperDARN coverage in different years and to exclude the inaccuracy caused by extended convection patterns, the mid-latitude radars data are not included. The selected radars are shown in Fig. 1a. Shadow colored areas are the field of view of radars, blue represents high-latitude radar, green is polar cap radar. The red circle marks the geomagnetic latitude at 60°.

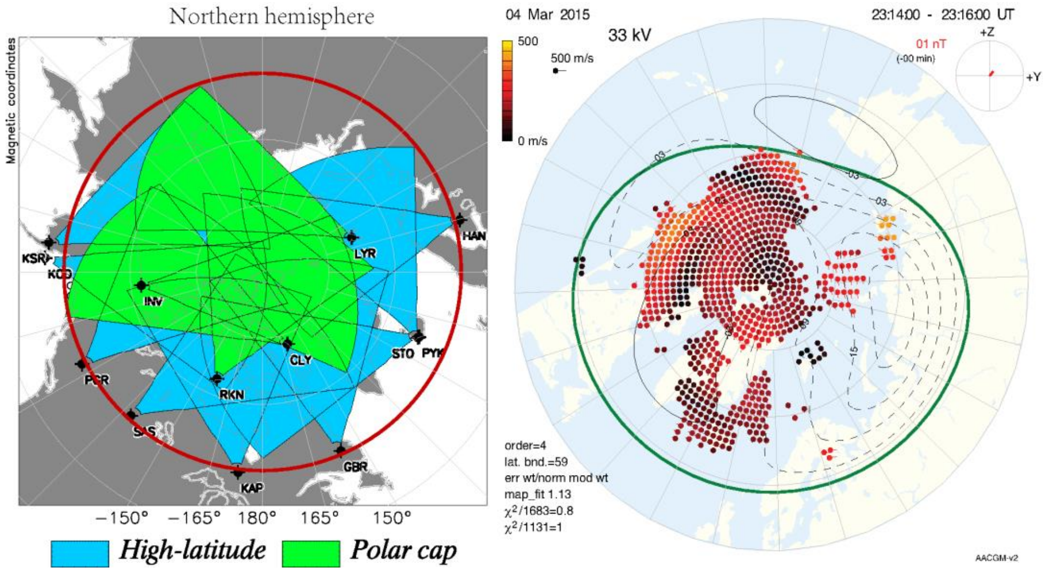

Fig. 1. SuperDARN radar coverages and an example map during the radial IMF. (a) Radar coverages. (b) An example HMB map. The solid green line is the HMB for this map, and the midnight latitude is 59°.

We use the Radar Software Toolkit 4.2 (RST4.2)， a free authorized and powerful software to process SuperDARN data (Barnes & Greenwald, 2005)， to calculate the HMB boundary from radars' rawacf data. Here we use a standard criterion to determining the HMB (Imber et al., 2013a): the velocity threshold is set for $100m/s$, and the number threshold of the effective radar backscatter points in a convection map is 150. Thus, HMB can be obtained every 2 min.

A convection map on the northern hemisphere during a typical radial IMF condition is shown in Fig. 1b. The convection map is calculated from the averaged radar data assigned to a 2min scan period (2015-03-04 23:14UT-23:16UT). Magnetic local noon locates to the top of the figure and dusk is to the left. The colored scatters represent fitted ionospheric echoes from radar observations, with the color and the vector direction corresponding to the velocity of the plasma flow given by the fourth-order spherical harmonic fit. The dashed and solid black lines depict the electrostatic potential, the contours of constant electrostatic potential also represent plasma flow streamlines for the whole polar ionosphere. The right upper corner marks the IMF condition, which shows noticeable small B_Y and B_Z. The solid green line is the HMB for this map constraining the extent of the mapping, and its midnight latitude is 59°. Based on the above criterion, we calculate all the HMB maps between 2002 and 2017, and our database can be seen in the appendix.

3.Statistical results and discussion

We average the HMB midnight latitudes for each radial IMF event for the northern hemisphere and then get 2292 data in total. Fig. 2 is the distribution of the HMB midnight latitudes. The x-axis is midnight latitude and the y-axis is the number of events. n represents the number of total events, the red (green) numeric value is mean (median) value for each panel. Fig. 2a shows HMB latitudes for anti-sunward B_X on the northern hemisphere. Event number, mean and median values of the HMB at midnight are 1063, 65.59 and 65.57, respectively. Fig. 2b gives the HMB latitudes in sunward B_X. The corresponding event number, mean and median are 1229, 65.83 and 65.71, respectively. The red line in each panel marks a Gauss Fitting Curve.

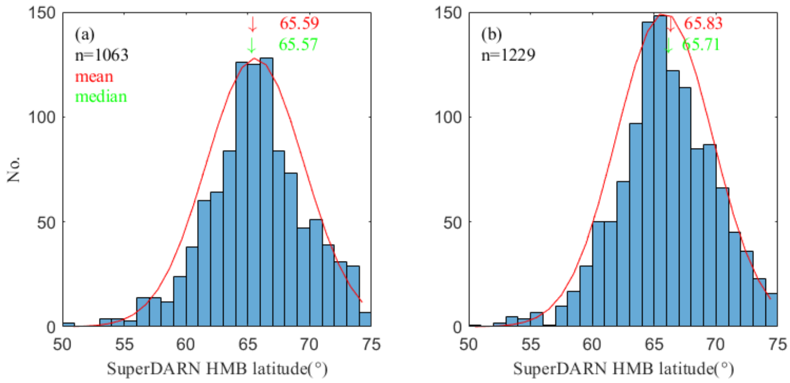

Fig. 2. The distribution of the HMB midnight latitudes. n is the number of total events, the red/green numeric value is the mean/median for each panel. (a) HMB latitudes in anti-sunward radial, (b) HMB latitudes in sunward radial.

It is shown that, under the radial IMF condition, the majority distributions of HMB midnight latitude is around 65.57°-65.83°, which are apparently higher than the average value of 63.1° for the substorm periods revealed by Imber et al. (2013b), and also larger than the average of 64° for the time period from January 1996 to August 2012 as shown in Imber et al. (2013a). This result signifies that during radial IMFs, ionospheric convection pattern is smaller. It suggests that the energy coupling efficient inputting from the solar wind into the magnetosphere is evidently weak. This is consistent with our understanding of the radial IMF, whose driving effect is weak (compared with southward IMF). The HMB midnight latitude for anti-sunward radial IMF is smaller than that in the sunward radial IMF. It suggests that the anti-sunward radial IMF injects more energy into the ionosphere. The difference of topological structure between anti-sunward and sunward radial IMF in large scale S-M-I coupling can be seen in Fig3.

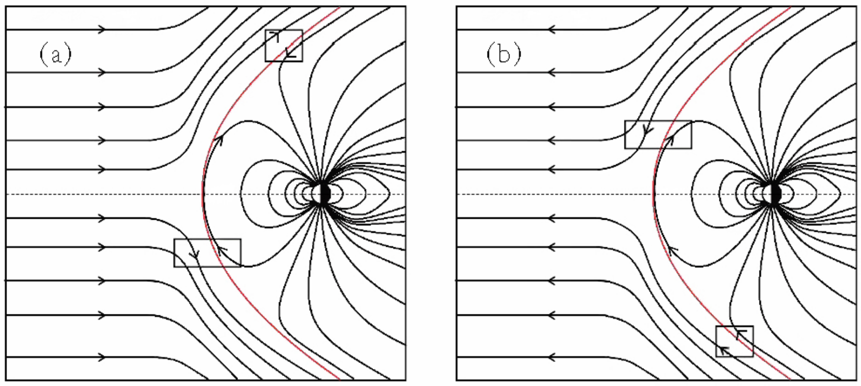

Fig. 3. Schematic illustration of the topological structure between IMF and magnetosphere. The red line indicates the boundary of the magnetosphere on dayside, the rectangles are possible locations of magnetic reconnection. (a) anti-sunward radial, (b) sunward radial.

Fig. 3 is a schematic illustration in the GSM X-Z plane showing the topological structure of radial events between the IMF and the magnetosphere. Fig. 3a (3b) shows the case of an anti-sunward (sunward) radial case. The black lines represent the magnetic field lines of the solar wind and the Earth. The red line marks the boundary of the magnetosphere on the dayside. The rectangles label possible locations of magnetic reconnection. A low-latitude reconnection and a single lobe reconnection can be found during a radial IMF. It is easy to understand that low-latitude reconnection contributes to both hemispheres while single lobe reconnection can only affect one hemisphere. In an ideal situation (zero for B_Z and B_Y), we assume that the transformation rate of B_X to B_Z equal in northern and southern hemispheres. Accordingly, we can infer that the low-latitude reconnection rates almost the same in Fig. 3a and 3b.

3.1 Correlation analysis

In S-M-I coupling, the magnetic field in local region of reconnection is an important parameter (e.g., Cassak & Shay, 2007). It is difficult to obtain the magnetic field characters in the local magnetosheath for all the time. In addition, due to the draping effect, IMF B_X component will be transformed into B_Z component in the magnetosheath (Pi et al., 2017). Therefore, for statistical study, the magnetic field in magnetosheath can be reflected by IMF B_X in radial IMF.

In this section, we discuss the correlation between HMB midnight latitude and B_X component during radial IMFs. Fig. 4 shows scatter plots of HMB midnight latitudes and B_X magnitude. The x-axis is HMB midnight latitude, and the y-axis is the strength of IMF B_X. R represents the Pearson correlation coefficient, SE_{cc} marks the standard deviation of correlation coefficient ($SE_{cc} = \sqrt{(1-R^2)/(n-2)}$, n means counts of events). The black line represents the linear fitting line and its corresponding expression is shown at the bottom of each panel. (e.g., in Fig. 4a left the HMB midnight latitude (x) and IMF B_X (y) satisfy $log\ (y)\ = 0.014x - 1.6$, and R (SE_{cc}) is 0.353 (0.029)). All anti-sunward radial events are shown in the left panel of Fig.4a, and the right figure gives all sunward radial events.

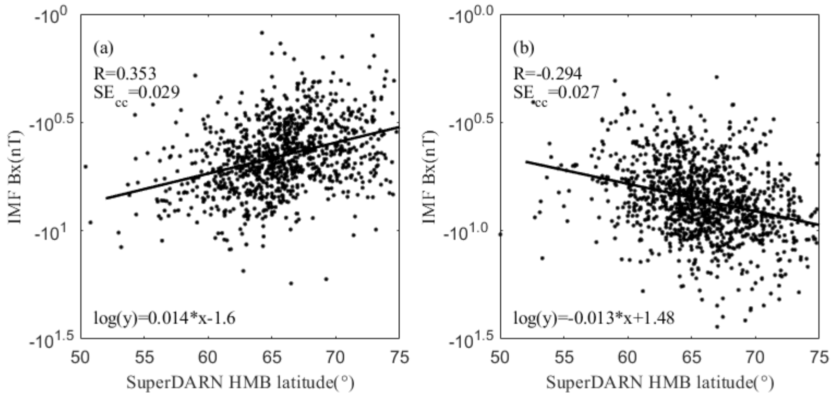

Fig. 4. The correlation between HMB midnight latitude and B_X. (a) all radial events in anti-sunward cases. (b) all radial events in sunward cases.

In both statistical classifications, a negative correlation between the strength of B_X and HMB midnight latitude can be found. The absolute value of the correlation coefficient with 0.353 in the anti-sunward radial IMF is larger than that in the sunward radial IMF (0.294). Two coefficients both show weak correlation, it suggested that B_X has relatively smaller contribution on the magnetic reconnection process. In addition, the AE index is very closed in two cases (anti-sunward 142.2; sunward 119.4), we can infer that difference in nightside reconnection rates is small. Therefore, difference in correlation coefficients is mainly caused by the asymmetric topological structure between the IMF and the magnetosphere (e.g., locations of rectangles on Fig. 3).

3.2 Seasonal effects

Previous studies have shown that the subsolar X-line location (the region where reconnection may occur) can shift poleward from the subsolar point, and the X-line location has a seasonal dependence (e.g., Trattner et al., 2007; Hoshi et al., 2018). This shift will undoubtedly affect the coupling process. In this section, we study the effect of seasonal variations on the correlation between IMF B_X and HMB midnight latitude.

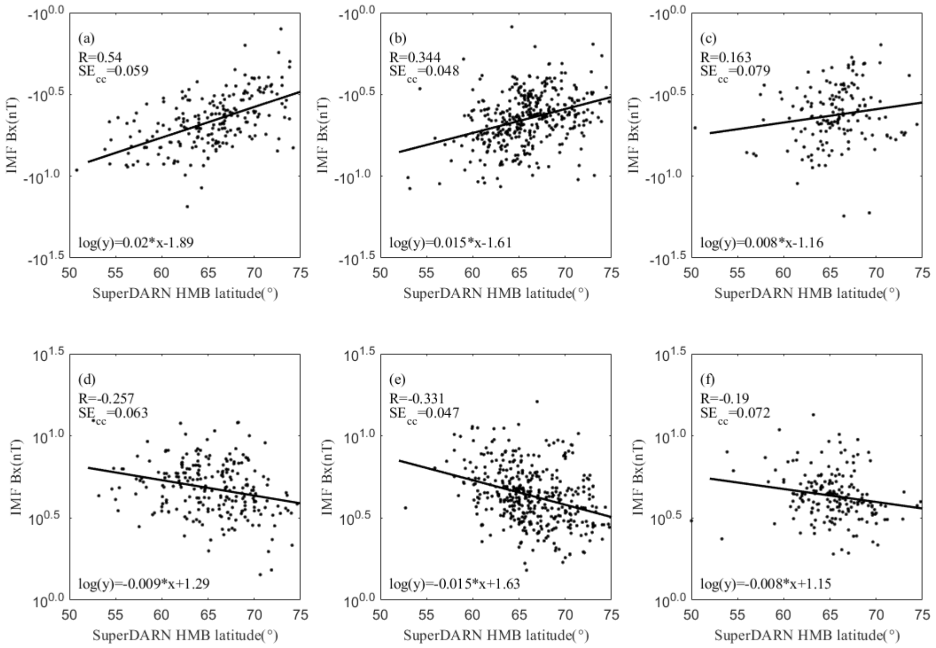

Fig. 5. seasonal variations. Top row is plots for anti-sunward radial events, and sunward radial events are shown in bottom row. The columns from left to right are radial events in winter, equinoxes and summer.

Fig. 5 shows the seasonal variations. In Fig.5 the top row is plots for anti-sunward radial events, and sunward radial events are shown in the bottom row. The columns from left to right are radial events in winter (Dec/Jan), equinoxes (Mar/Apr/Sep/Oct) and summer (Jun/Jul). The correlation varies significantly in different panels of Fig.5. The correlation in anti-sunward radial events between B_X and HMB midnight latitude is extremely high during wintertime, the coefficient is up to 0.54 (Fig. 5a). In this case, the effect of IMF B_X on HMB is very large for a chaotic system. Statistical results suggest that negative IMF B_X plays an important role in the S-M-I coupling process during wintertime. Top raw figures of Fig. 5 show that, with the northward shift of the subsolar point, the correlation coefficients in anti-sunward radial events become weaker from winter to summer. In the bottom figures of Fig. 5, for positive B_X events, the correlation coefficients become stronger with the equatorward moving of subsolar point. However, the correlation between positive B_X cases is weak in all seasons. As shown in right figures of Fig. 5, very weak correlation can be found in both directions of B_X during summertime. In summer, solar radiation has a great influence on the photoionization effect on the dayside ionosphere, which causes the enhancement of the dayside ionospheric conductivity. It is expected that the dayside R1 current will increase, accordingly, the magnetosphere shrinks on the dayside and expands on the nightside (Ohtani et al., 2014). The energy transmission from the solar wind to the Earth will be affected by the morphological structure change of magnetopause (Jing et al., 2014; Merkin et al., 2005; Ohtani et al., 2014; Raeder et al., 2001). That's the reason for a weaker correlation in summer.

For positive B_X events, the topological structure is similar to the southward IMF on the northern hemisphere. When the northern hemisphere is in summer (winter) and the north (south) pole tilts toward the Sun, the reconnection location under finite dipole tilt shifts toward the winter (summer) hemisphere (GSM coordinate) (Hoshi et al., 2018; Komar et al., 2014; Russell et al., 2003; Trenchi et al., 2008), and the reconnection rates can be reduced by this kind of X-line shift (Borovsky et al., 2008; Cassak & Shay, 2007). Furthermore, the SE_{cc} in each panel is small, which suggests that the correlation coefficients have enough credibility. Therefore, a negative correlation can be found between the correlation coefficient and the absolute value of subsolar point latitude in sunward radial.

It is more interesting in negative B_X events. It is not straightforward to explain why the anti-sunward radial events have such a high correlation in winter. We separate each negative B_X events in different seasons according to different directions of B_Z (positive, negative) and calculate the correlation coefficients respectively. The correlation coefficients for positive (negative) B_Z are listed as follows: winter 0.538 (0.567); equinoxes 0.205 (0.471). We can see that the effect of B_Z is more evident in equinoxes. As mentioned in section 1, due to the draping effect, the IMF B_X will be transformed into the magnetosheath magnetic field B_Z with different polarities on the southern and northern hemispheres. In simple geometric theory, when the transformation line with the same (opposite) direction as the IMF B_Z, the influence of IMF B_X will be larger (smaller). It suggests that the transformation is mainly near the middle plane, and mainly affects low latitude reconnection. The correlation coefficient shows almost the same in winter, which seems to indicate that the main reason for such large correlation coefficient in negative B_X events during wintertime is not due to the low latitude reconnection.

As shown in Fig. 3, in anti-sunward radial condition, the northern hemisphere will be affected by both low-latitude and single lobe reconnection. We check the averaged AE index values (winter 149.7; equinoxes 144.6), which suggests that the nightside reconnection rate is almost identical inferred from AE. As mentioned above, we speculate that the dramatically high correlation in anti-sunward radial condition during wintertime is mainly due to the effect of lobe reconnection. There are some issues with lobe reconnection. The energy transport related to lobe reconnection is usually much less than the one associated with the low latitude magnetopause reconnection, the related region is also much smaller, usually limited to above 80◦ MLAT on the dayside (06–18 MLT) in the ionospheric height (Reistad et al., 2019). With the enhancement of ionospheric conductivity, the lobe reconnection rate increases correspondingly (Paschmann et al., 2003; Reistad et al., 2019). This indicates that although single lobe reconnection cannot produce open magnetic lines (Imber et al., 2006), the special configuration between the magnetopause and solar wind during anti-sunward radial period seems to have a great impact on lobe reconnection rate during wintertime and inject much energy into the polar ionosphere. What occurred for anti-sunward radial in winter time on northern hemisphere is interesting and not confirmed. We will take a further study on this issue in future work.

4. Summary and expectation

In this study, we select radial IMF events to study the correlation between IMF B_X component and HMB, because the radial IMF can ideally ignore most of the other factors. The main findings in this work can be summarized as follows:

1. The solar wind is continuously stable and weak during radial IMF, and under this condition, HMB midnight latitude is higher than that during both long-term period (1997-2012) and high geomagnetic activity cases (Imber et al., 2013a, 2013b).
2. B_X has a small effect on the coupling process, and a negative correlation can be found between the strength of B_X and HMB midnight latitude. The correlation coefficient in the northern hemisphere is only 0.29~0.35.
3. During northern hemispheric wintertime, the correlation coefficient between the strength of B_X and HMB midnight latitude is up to 0.54 in anti-sunward radial events. In such situation, the effect of B_X in the coupling process is important and can't be ignored.
4. When the direction of the magnetic field line in magnetosheath is antiparallel to that of the geomagnetic field line in the low latitudes and parallel in the lobe region, the correlation coefficients is larger in equinoxes, but is smaller during the winter and summer. When the magnetic field direction in magnetosheath is anti-parallel with the geomagnetic field in low latitudes and also anti-parallel in the lobe region, a negative correlation between correlation coefficients and latitude of subsolar point can be found.

As a statistical study, we find an abnormal large correlation coefficient between B_X and HMB in the winter northern hemisphere when B_X is negative. Although we present a possible explanation, further research is needed.

Acknowledgments

We acknowledge the use of NASA/GSFC's Space Physics Data Facility (https://omniweb.gsfc.nasa.gov/html/HROdocum.html) for OMNI IMF data. SuperDARN (http://vt.superdarn.org/tikiindex.php) is an international collaboration involving more than 30 low-power HF radars that are operated and funded by universities and research organizations in Australia, Canada, China, France, Italy, Japan, Norway, South Africa, the United Kingdom, and the United States. We thank PRIC (http://www.pric.org.cn) for providing a computing server and SuperDARN data. Raw files can also be accessed via the SuperDARN data mirrors hosted by the British Antarctic Survey (https://www.bas.ac.uk/project/superdarn/#data) and University of Saskatchewan (https://superdarn.ca). This work was supported in part by the National Key Research and Development Plan of China (2018YFC1407305, 2018YFC1407304, 2018YFF01013706), the National Natural Science Foundation of China (grant 41974190, 41431072, 41974185, 41574158, 41831072, 41674169, U1631107), the Foundation of National Key Laboratory of Electromagnetic Environment (201801003), the Natural Science Foundation of Jiangsu Province (BK20170952) and the Chinese Meridian Project.

Reference

Akasofu, S.-I. (1981). Energy coupling between the solar wind and the magnetosphere. Space Science Reviews, 28(2), 121–190.

Barnes, R. ~J., & Greenwald, R. (2005). The Radar Software Toolkit: Anaylsis software for the ITM community. In AGU Spring Meeting Abstracts (Vol. 2005, pp. SH51B-11).

Belenkaya, E. S. (1998). High-latitude ionospheric convection patterns dependent on the variable imf orientation. Journal of Atmospheric and Solar-Terrestrial Physics, 60(13), 1343–1354.

Boakes, P. D., Milan, S. E., Abel, G. A., Freeman, M. P., Chisham, G., Hubert, B., & Sotirelis, T. (2008). On the use of IMAGE FUV for estimating the latitude of the open/closed magnetic field line boundary in the ionosphere. Annales Geophysicae, 26(9), 2759–2769.

Borovsky E., J. (2008). The rudiments of a theory of solar wind/magnetosphere coupling derived from first principles. Journal of Geophysical Research: Space Physics, 113(8), 1–14.

Borovsky, J. E., Hesse, M., Birn, J., & Kuznetsova, M. M. (2008). What determines the reconnection rate at the dayside magnetosphere? Journal of Geophysical Research: Space Physics, 113(7), 1–17.

Cassak, P. A., & Shay, M. A. (2007). Scaling of asymmetric magnetic reconnection: General theory and collisional simulations. Physics of Plasmas, 14(10), 1–11.

Dungey, J. W. (1961). Interplanetary magnetic field and the auroral zones. Physical Review Letters, 6(2), 47–48.

Grocott, A., & Milan, S. E. (2014). The influence of IMF clock angle timescales on the morphology of ionospheric convection. Journal of Geophysical Research: Space Physics, 119(7), 5861–5876.

Heppner, J. P., & Maynard, N. C. (1987). Empirical high-latitude electric field models. Journal of Geophysical Research, 92(A5), 4467.

Hoshi, Y., Hasegawa, H., Kitamura, N., Saito, Y., & Angelopoulos, V. (2018). Seasonal and Solar Wind Control of the Reconnection Line Location on the Earth's Dayside Magnetopause. Journal of Geophysical Research: Space Physics, 123(9), 7498–7512.

Imber, S. M., Milan, S. E., & Hubert, B. (2006). The auroral and ionospheric flow signatures of dual lobe reconnection. Annales Geophysicae, 24(11), 3115–3129.

Imber, S. M., Milan, S. E., & Lester, M. (2013a). Solar cycle variations in polar cap area measured by the superDARN radars. Journal of Geophysical Research: Space Physics, 118(10), 6188–6196.

Imber, S. M., Milan, S. E., & Lester, M. (2013b). The Heppner-Maynard Boundary measured by SuperDARN as a proxy for the latitude of the auroral oval. Journal of Geophysical Research: Space Physics, 118(2), 685–697.

Jing, H., Lu, J. Y., Kabin, K., Zhao, J. S., Liu, Z. Q., Yang, Y. F., et al. (2014). MHD simulation of energy transfer across magnetopause during sudden changes of the IMF orientation. Planetary and Space Science, 97, 50–59.

Kabin, K., Rankin, R., Rostoker, G., Marchand, R., Rae, I. J., Ridley, A. J., et al. (2004). Open-closed field line boundary position: A parametric study using an MHD model. Journal of Geophysical Research: Space Physics, 109(A5), 1–10.

Kan, J. R., & Lee, L. C. (1979). Energy coupling function and solar wind-magnetosphere dynamo. Geophysical Research Letters, 6(7), 577–580.

Komar, C. M., Fermo, R. L., & Cassak, P. A. (2014). Journal of Geophysical Research : Space Physics Comparative analysis of dayside magnetic reconnection, 1–19.
Lockwood, M. (1998). Identifying the Open-Closed Field Line Boundary. Polar Cap Boundary Phenomena, 73–90.
Lu, J. Y., Jing, H., Liu, Z. Q., Kabin, K., & Jiang, Y. (2013). Energy transfer across the magnetopause for northward and southward interplanetary magnetic fields. Journal of Geophysical Research: Space Physics, 118(5), 2021–2033.
Lu, J. Y., Zhang, H., Wang, M., Gu, C., & Guan, H. (2019). Magnetosphere response to the IMF turning from north to south. Earth and Planetary Physics, 3(1), 8–16.
Merkin, V. G., Sharma, A. S., Papadopoulos, K., Milikh, G., Lyon, J., & Goodrich, C. (2005). Global MHD simulations of the strongly driven magnetosphere: Modeling of the transpolar potential saturation. Journal of Geophysical Research: Space Physics, 110(A9), 1–11.
Milan, S. E., Provan, G., & Hubert, B. (2007). Magnetic flux transport in the Dungey cycle: A survey of dayside and nightside reconnection rates. Journal of Geophysical Research: Space Physics, 112(1), 1–13.
Milan, S. E., Gosling, J. S., & Hubert, B. (2012). Relationship between interplanetary parameters and the magnetopause reconnection rate quantified from observations of the expanding polar cap. Journal of Geophysical Research: Space Physics, 117(3), 1–16.
Murr, D. L., & Hughes, W. J. (2007). The coherence between the IMF and high-latitude ionospheric flows: The dayside magnetosphere-ionosphere low-pass filter. Journal of Atmospheric and Solar-Terrestrial Physics, 69(3), 223–233.
Newell, P. T., Sotirelis, T., Liou, K., Meng, C. I., & Rich, F. J. (2007). A nearly universal solar wind-magnetosphere coupling function inferred from 10 magnetospheric state variables. Journal of Geophysical Research: Space Physics, 112(1), 1–16.
Ohtani, S., Wing, S., Merkin, V. G., & Higuchi, T. (2014). Solar cycle dependence of nightside field-aligned currents: Effects of dayside ionospheric conductivity on the solar wind-magnetosphere-ionosphere coupling. Journal of Geophysical Research: Space Physics, 119(1), 322–334.
Paschmann, G., Haaland, S., & Treumann, R. (Eds.). (2003). Auroral Plasma Physics. Dordrecht: Springer Netherlands.
Peng, Z., Wang, C., & Hu, Y. Q. (2010). Role of IMF Bx in the solar wind-magnetosphere-ionosphere coupling. Journal of Geophysical Research: Space Physics, 115(8), 1–7.
Pi, G., Shue, J.-H., Chao, J.-K., Němeček, Z., Šafránková, J., & Lin, C.-H. (2014). A reexamination of long-duration radial IMF events Gilbert. Journal of Geophysical Research: Space Physics, 119(7), 7005–7011.
Pi, G., Shue, J. H., Grygorov, K., Li, H. M., Němeček, Z., Šafránková, J., et al. (2017). Evolution of the magnetic field structure outside the magnetopause under radial IMF conditions. Journal of Geophysical Research: Space Physics, 122(4), 4051–4063.
Rae, I. J., Kabin, K., Rankin, R., Fenrich, F. R., Liu, W., Wanliss, J. A., et al. (2004). Comparison of photometer and global MHD determination of the open-closed field line boundary. Journal of Geophysical Research: Space Physics, 109(A1), 1–9.
Raeder, J., Wang, Y. L., Fuller-Rowell, T. J., & Singer, H. J. (2001). Global simulation of magnetospheric space weather effects of the Bastille day storm.

Solar Physics, 204(1–2), 325–338.
Reistad, J. P., Laundal, K. M., Østgaard, N., Ohma, A., Thomas, E. G., Haaland, S., et al. (2019). Separation and Quantification of Ionospheric Convection Sources: 2. The Dipole Tilt Angle Influence on Reverse Convection Cells During Northward IMF. Journal of Geophysical Research: Space Physics.
Russell, C. T., Wang, Y. L., & Raeder, J. (2003). Possible dipole tilt dependence of dayside magnetopause reconnection. Geophysical Research Letters, 30(18), 2–5.
Scurry, L., & Russell, C. T. (1991). Proxy studies of energy transfer to the magnetosphere. Journal of Geophysical Research, 96(A6), 9541.
Suvorova, A. V., Shue, J. H., Dmitriev, A. V., Sibeck, D. G., McFadden, J. P., Hasegawa, H., et al. (2010). Magnetopause expansions for quasi-radial interplanetary magnetic field: THEMIS and Geotail observations. Journal of Geophysical Research: Space Physics, 115(10), 1–16.
Tang, B. B., Wang, C., & Li, W. Y. (2013). The magnetosphere under the radial interplanetary magnetic field: A numerical study. Journal of Geophysical Research: Space Physics, 118(12), 7674–7682.
Temerin, M., & Li, X. (2006). Dst model for 1995-2002. Journal of Geophysical Research: Space Physics, 111(4), 1–11.
Thomas, E. G., & Shepherd, S. G. (2018). Statistical Patterns of Ionospheric Convection Derived From Mid-latitude, High-Latitude, and Polar SuperDARN HF Radar Observations. Journal of Geophysical Research: Space Physics, 123(4), 3196–3216.
Trattner, K. J., Mulcock, J. S., Petrinec, S. M., & Fuselier, S. A. (2007). Location of the reconnection line at the magnetopause during southward IMF conditions. Geophysical Research Letters, 34(3), 1–5.
Trenchi, L., Marcucci, M. F., Pallocchia, G., Consolini, G., Bavassano Cattaneo, M. B., Di Lellis, A. M., et al. (2008). Occurrence of reconnection jets at the dayside magnetopause: Double Star observations. Journal of Geophysical Research: Space Physics, 113(7), 1–13.
Vasyliunas, V. M., Kan, J. R., Siscoe, G. L., & Akasofu, S. I. (1982). Scaling relations governing magnetospheric energy transfer. Planetary and Space Science, 30(4), 359–365.
Wang, C., Wang, J. Y., Lopez, R. E., Zhang, L. Q., Tang, B. B., Sun, T. R., & Li, H. (2014). Effects of the interplanetary magnetic field on the twisting of the magnetotail: Global MHD results. Journal of Geophysical Research: Space Physics, 119(3), 1887–1897.
Wygant, J. R., Torbert, R. B., & Mozer, F. S. (1983). Comparison of S3-3 Polar Cap Potential Drops With the Interplanetary Magnetic Field and Models of Magnetopause Reconnection. Journal of Geophysical Research, 88(A7), 5727–5735.

Figure 1.

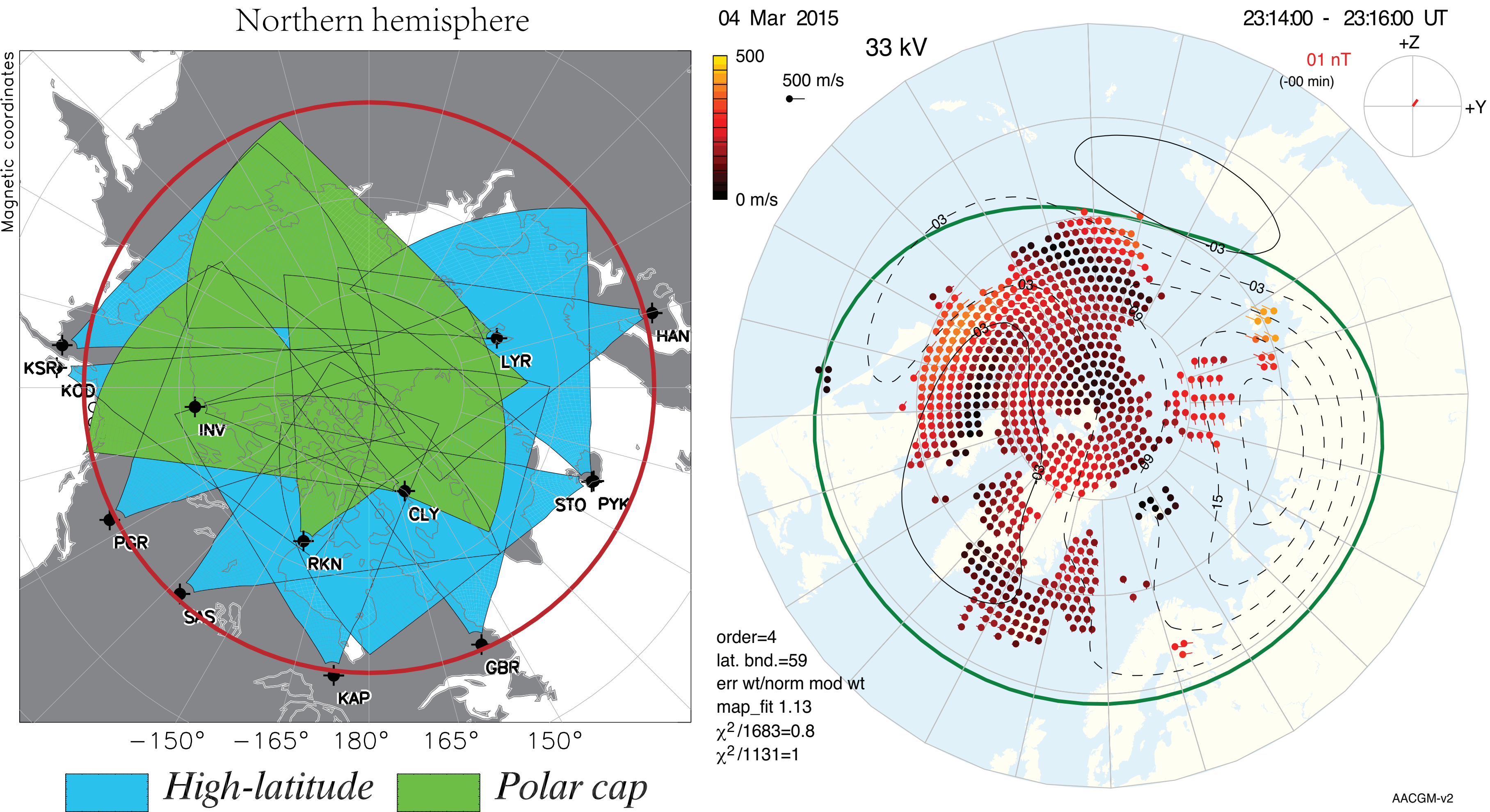

Northern hemisphere
Magnetic coordinates
KSR
KOD
INV
LYR
HAN
PGR
RKN
CLY
STO
PYK
SAS
KAP
GBR
−150°
−165°
180°
165°
150°
High-latitude
Polar cap
04 Mar 2015
23:14:00 - 23:16:00 UT
33 kV
500
0 m/s
500 m/s
01 nT
(-00 min)
+Z
+Y
order=4
lat. bnd.=59
err wt/norm mod wt
map_fit 1.13
χ2/1683=0.8
χ2/1131=1
AACGM-v2

Figure 2.

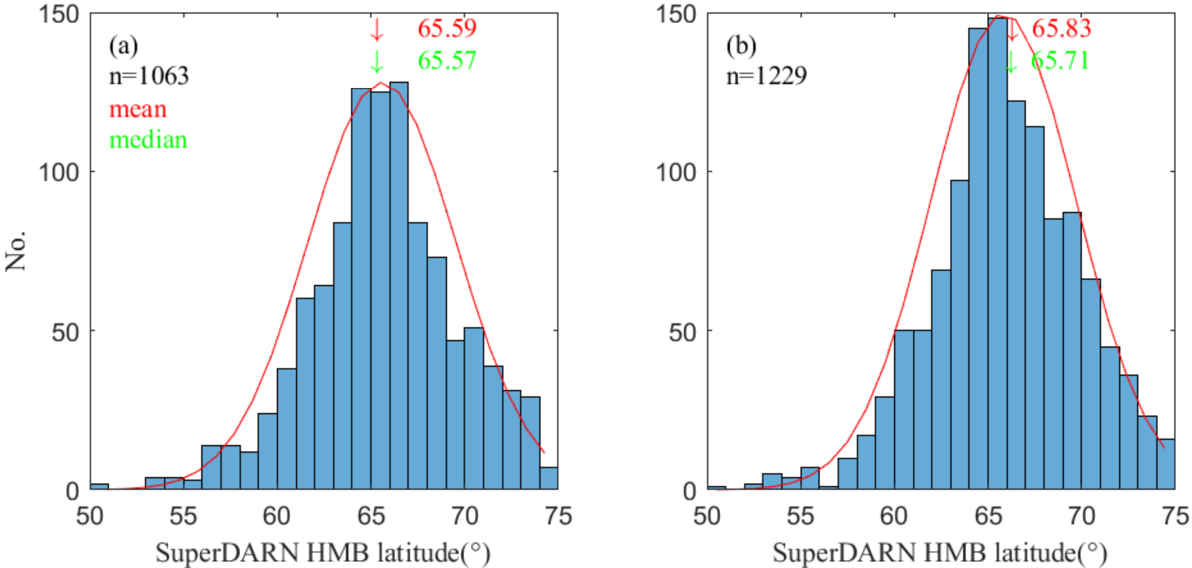
(a)
n=1063
mean
median
65.59
65.57
No.
SuperDARN HMB latitude(°)
(b)
n=1229
65.83
65.71
SuperDARN HMB latitude(°)
150
100
50
0
50
55
60
65
70
75

Figure 3.

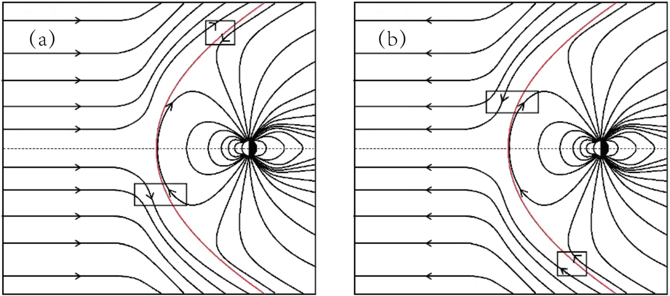
(a)
(b)

Figure 4.

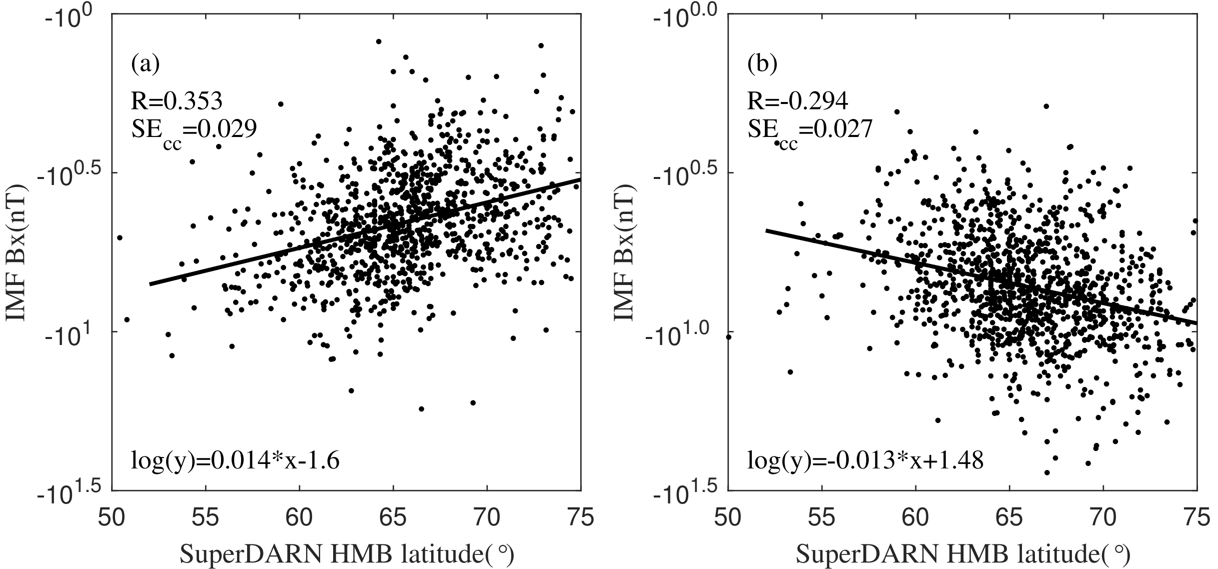
(a)
R=0.353
SE_cc=0.029
log(y)=0.014*x-1.6
IMF Bx(nT)
SuperDARN HMB latitude(°)
(b)
R=-0.294
SE_cc=0.027
log(y)=-0.013*x+1.48
IMF Bx(nT)
SuperDARN HMB latitude(°)

Figure 5.

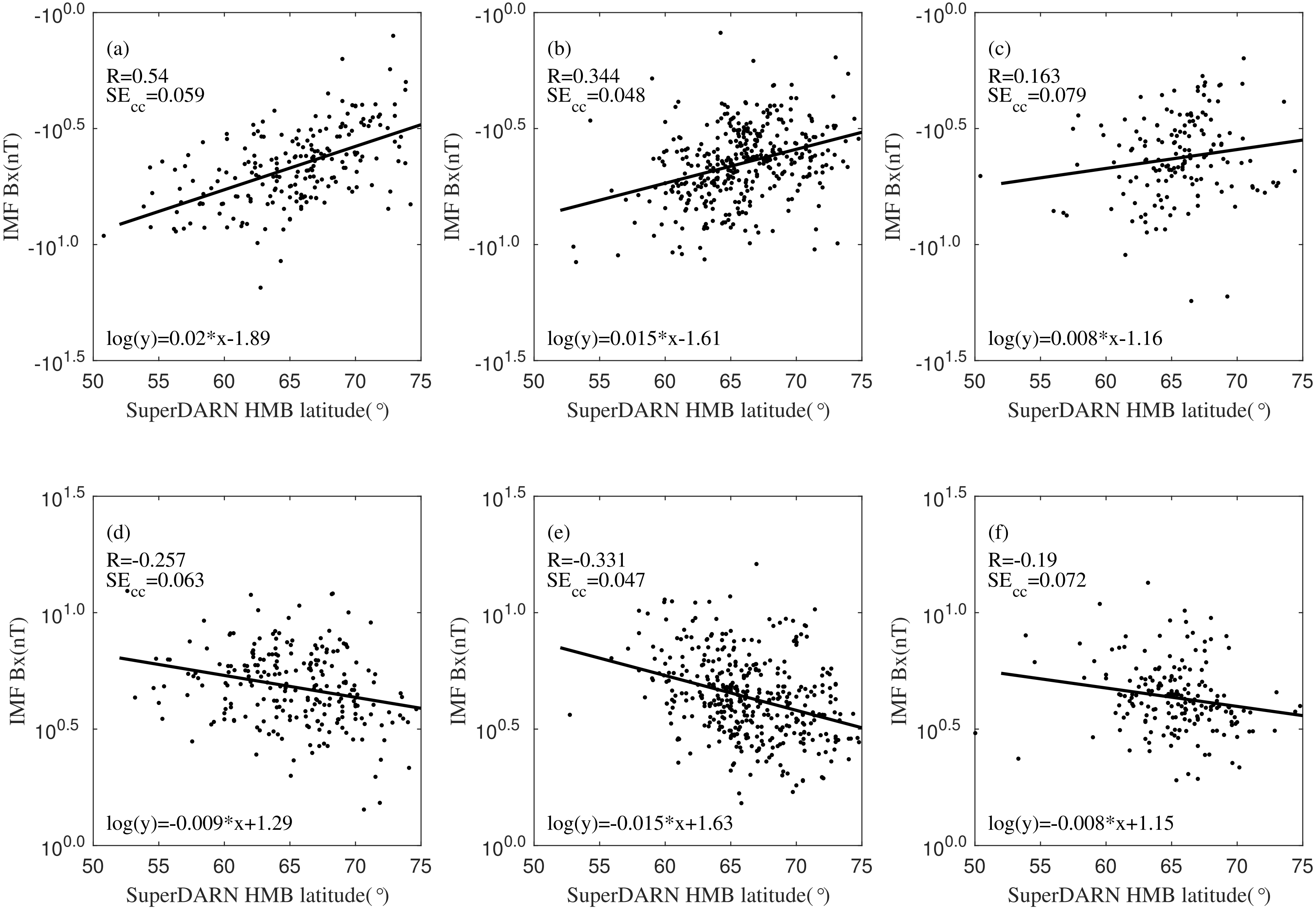

(a)
R=0.54
SEcc=0.059
log(y)=0.02*x-1.89
(b)
R=0.344
SEcc=0.048
log(y)=0.015*x-1.61
(c)
R=0.163
SEcc=0.079
log(y)=0.008*x-1.16
(d)
R=-0.257
SEcc=0.063
log(y)=-0.009*x+1.29
(e)
R=-0.331
SEcc=0.047
log(y)=-0.015*x+1.63
(f)
R=-0.19
SEcc=0.072
log(y)=-0.008*x+1.15
IMF Bx(nT)
SuperDARN HMB latitude(°)